JACS
JOURNAL OF THE AMERICAN CHEMICAL SOCIETY
pubs.acs.org/JACS
Article

Investigations of Molecular Optical Properties Using Quantum Light and Hong–Ou–Mandel Interferometry

Audrey Eshun, Bing Gu, Oleg Varnavski, Shahaf Asban, Konstantin E. Dorfman, Shaul Mukamel, and Theodore Goodson, III*

Cite This: J. Am. Chem. Soc. 2021, 143, 9070–9081
Read Online
ACCESS | Metrics & More | Article Recommendations | Supporting Information

ABSTRACT: Entangled photon pairs have been used for molecular spectroscopy in the form of entangled two-photon absorption and in quantum interferometry for precise measurements of light source properties and time delays. We present an experiment that combines molecular spectroscopy and quantum interferometry by utilizing the correlations of entangled photons in a Hong–Ou–Mandel (HOM) interferometer to study molecular properties. We find that the HOM signal is sensitive to the presence of a resonant organic sample placed in one arm of the interferometer, and the resulting signal contains information pertaining to the light–matter interaction. We can extract the dephasing time of the coherent response induced by the excitation on a femtosecond time scale. A dephasing time of 102 fs is obtained, which is relatively short compared to times found with similar methods and considering line width broadening and the instrument entanglement time As the measurement is done with coincidence counts as opposed to simply intensity, it is unaffected by even-order dispersion effects, and because interactions with the molecular state affect the photon correlation, the observed measurement contains only these effects and no other classical losses. The experiments are accompanied by theory that predicts the observed temporal shift and captures the entangled photon joint spectral amplitude and the molecule's transmission in the coincidence counting rate. Thus, we present a proof-of-concept experimental method based of entangled photon interferometry that can be used to characterize optical properties in organic molecules and can in the future be expanded on for more complex spectroscopic studies of nonlinear optical properties.

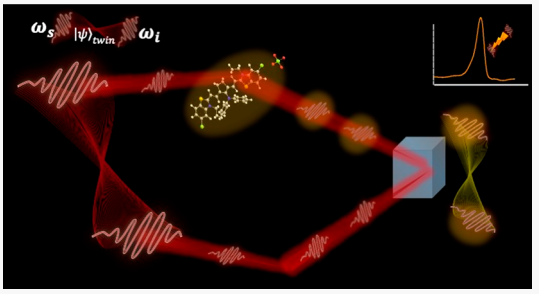

I. INTRODUCTION

Our growing understanding of quantum light over the years has led researchers to utilize its unique properties toward advancements in quantum information science, in the fields of computing, cryptography, imaging, and quantum sensing.[1−4] Of particular interest has been the subject of spectroscopy with quantum light, as it offers avenues to overcome classical Fourier limitations, the opportunity for enhanced light–matter coupling due to its distinct photon statistics, and novel control knobs defined by the quantum photon field wave function. So far, quantum light spectroscopy has been approached experimentally with entangled two-photon absorption studies[5−16] via absorption, fluorescence, and microscopy. These measurements have provided great progress with enhanced resolution in two-photon cross-section measurements as well as the ability to conduct spectroscopy at extremely low light intensities, limiting the risk of damaging the studied sample. We now wish to develop experimental quantum light spectroscopy even further. In this work, by exploiting the correlations of entangled photon pairs via two-photon interferometry, we seek to illustrate a new method of spectroscopy to study molecular properties using a Hong–Ou–Mandel (HOM) setup, which has not yet been used to probe molecules experimentally in such a way.

Because of the unique quantum interference properties of the HOM phenomenon, it presents itself as an interesting and robust outlet for investigating quantum light–matter interactions. We have designed and set up an experiment where as a result of the quantum interference of the indistinguishable photons we observe the effect the sample's presence in the interferometer path has on the light's photon statistics as opposed to simply the intensity, which provides information about the light statistics as well as features of the light–matter interactions. Being able to utilize interferometric schemes to detect linear and nonlinear susceptibilities with quantum light can improve the accuracy of our measurements of these material susceptibilities due to the increased sensitivity of quantum interferometers.[17,18] Furthermore, the susceptibilities

Received: March 8, 2021
Published: June 14, 2021

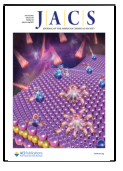

https://doi.org/10.1021/jacs.1c02514
J. Am. Chem. Soc. 2021, 143, 9070–9081

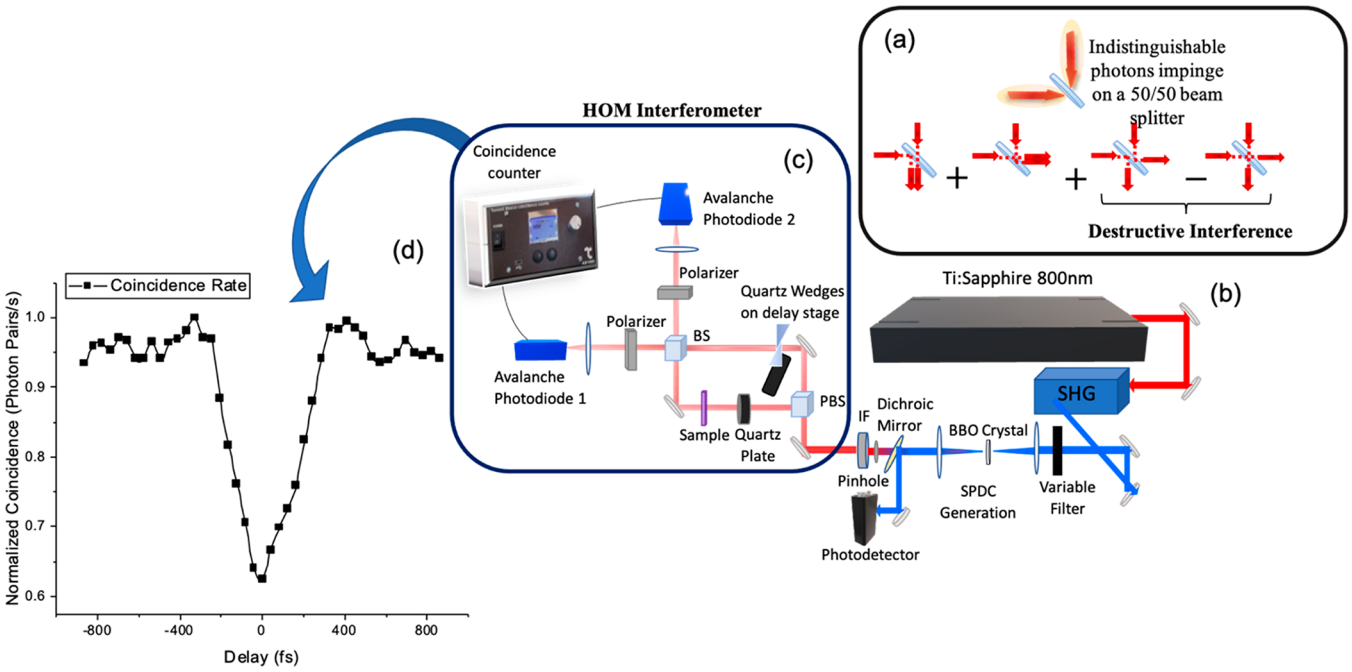

Figure 1. HOM pathways, SPDC generation, and HOM interferometer setup. (a) Schematic of possible Hong−Ou−Mandel (HOM) interferometer pathways. Indistinguishable photons are incident on a 50:50 beam splitter from orthogonal directions, and each photon is either reflected or transmitted. In the first two pathways, one photon is reflected and one transmitted, and coincidence counts are detected. In the last two pathways, both photons are either transmitted or reflected, leading to destructive interference and null coincidence counts. (b) Femtosecond laser and SPDC generation with type II SPDC BBO crystal. (c) Scheme of HOM interferometer. Entangled photon pair separated by a polarizing beam splitter. A molecular sample is placed in one arm and a delay line in the other, before beams recombine at a beam splitter. (d) HOM dip measured without sample. Coincidence counts are shown as a function of time delay.

can be connected to other physical properties of the matter such as coherence dephasing times, and in this article, we seek to make this connection through theory and extract the molecule's dephasing time from experimental data. This experimental scheme presents a novel and accessible way in which we can measure molecular optical properties with quantum light and serves as a model to be expanded on and adapted for future more complex spectroscopic studies. While the setup of an interferometer can be tedious, it is far less daunting and less involved than large expensive femtosecond laser systems usually used for time-resolved ultrafast or high-resolution spectroscopy. Improvements have been made in the field of quantum optics making the building of such HOM interferometers accessible to many researchers.[19−22] Thus, this straightforward interferometric setup can be used in place of complex laser systems to interrogate the dynamics of and interactions between molecular states with the advantages of quantum light.[23] As the interest in entangled light applications grows and more studies consider the possibility of utilizing it for spectroscopy,[23−26] we present experimental confirmation of a method that can be expanded into various fields that require sensitive spectroscopy of molecules.

The phenomenon of quantum interference with entangled light states is well understood and has been utilized in quantum optics mainly for metrology and quantum light characterization.[27] The nonclassical properties of photon pairs generated from spontaneous parametric downconversion (SPDC) allow them to be used for a variety of interferometric purposes such as the Hanbury Brown−Twiss[28] (HBT) and HOM interferometers. The HOM interferometer is a two-photon interference effect that measures the indistinguishability of photon pairs.[29] This two-photon interference at a beam splitter was initially exhibited by Hong, Ou, and Mandel in 1987[29] and Shih and Alley[30] and has been used in testing nonlocality, Bell-state measurements, and quantum metrology and in building quantum optical logical gates.[31] An HOM interferometer measures the quantum interference resulting from the interference of probability amplitudes of four different two-photon Feynman paths, when indistinguishable photons are incident on a 50/50 beam splitter (Figure 1a). When indistinguishable photons arrive simultaneously in time, they destructively interfere, leading to null coincidence counts at two detectors connected in coincidence. The temporal width of the resulting dip is the inverse of the bandwidth of the SPDC spectrum and the coherence time of the entangled photons.

While the presence of a simple refractive or birefringent material in the interferometer pathway can lead to polarization mode dispersion which degrades entanglement and causes temporal delays,[32] it is theorized that the presence of an absorbing material in an interferometer would result in a much more complex modification to the coincidence signal.[33,34] Such experiments with entangled light interferometers have been proposed.[23,35,36] One study was performed on inorganic crystals where Kalashnikov et al.[37] used a similar experimental outlook to conduct time-resolved measurements focused on coherent dynamics of inorganic nanostructures.[37] The study's focus was on the ability to use entangled photons for measurements of a medium's dephasing time with the HOM dip. However, their work considered solid crystals and nanostructures which are much easier to probe. In our work, we assess the sensitivity of the experimental setup and possibility of expanding it into more fields by conducting measurements on organic molecular chromophores. Changes

https://doi.org/10.1021/jacs.1c02514
J. Am. Chem. Soc. 2021, 143, 9070−9081

caused by molecules that are at unsaturated concentrations and do not have molecular aggregates will be more subtle; therefore, the HOM signal must be shown to be perceptible to these light−matter interactions. Furthermore, the inorganic crystals used in ref 35 have narrow resonances whereas the typical line widths of organic and biological systems are much broader. For such crystals, homogeneous broadening dominates inhomogeneous effects, and therefore it is easier to account for any slight changes caused by inhomogeneous broadening. By conducting the experiment with an organic chromophore, we show that the dephasing time can still be extracted despite the greater inhomogeneous broadening effects in organic molecules. In the case of our experiment, the SPDC spectrum is narrower than the molecule's line width. Thus, we show that subtle changes caused by organic chromophores can be perceived by our experiment and that information can be extracted even when the SPDC spectrum is narrower than the molecule's line width.

In our experiment, a resonant absorbing medium is placed in the signal arm of the interferometer. The signal beam transmits through the sample and subsequently becomes modified by its susceptibility ($\chi^{(1)}$), acquiring a phase shift for the different frequency components which introduces a delay in the signal mode. The idler beam undergoes a frequency-independent phase shift, compensating for the shift caused by the molecular interaction which introduces a time shift to the observed HOM dip upon recombination and interference of the signal and idler beams at the beam splitter. As there is quantum interference between the signal beam and the molecular states, the idler is not able to fully compensate for the acquired modification, and hence, there is a change in the shape of the HOM dip, i.e., loss of its symmetry. The molecule-induced modifications to the signal mode are frequency-dependent as encoded in ($\chi^{(1)}$); thus, the interaction with the sample breaks the exchange symmetry. Upon coherent excitation of the sample, the phase acquired by the propagating photons and corresponding group delay contribution leads to an asymmetry of the HOM dip that lasts for the duration related to T_2 for single resonance in absorption. Therefore, measuring the asymmetry caused by the group velocity may provide a measurement of the dephasing time. A longer asymmetric tail for the HOM picture will correspond to a longer T_2 for a single resonance.

The indistinguishable biphoton pair has a commutation relation that should equal zero at full indistinguishability.[38] As well described by Szoke et al.,[38] spectroscopy using HOM interference should measure how entangled light−matter interactions from a sample in the interferometer path will modify the commutation relation.[38] In that regard, the correlations between the photon pair are affected; the time at which the photons of the entangled pair overlap is shifted, and our measurements taken as a function of time allow us to obtain time-resolved data pertaining to the sample. Moreover, measurements of coincidence counts take into account changes of one photon with respect to its conjugate photon. Therefore, we measure alterations caused by the material as the interaction affects the statistics and indistinguishability of the photon pair. Because we measure the photon correlations, we are ensured that any observations are a result of the light−matter interaction only. Similar to advantages offered by entangled photons in other interferometric setups like quantum polarized light microscopy and quantum optical coherence tomography,[39] the two-photon N00N state is more phase sensitive[18] than classical counterparts; thus, our experimental HOM interference method should offer a quantum advantage with fewer sources of systematic errors with fewer photons.[18] In addition to the benefits of low intensity and lower noise that can be achieved by using entangled photons, this quantum interferometry setup has the advantage of being able to probe optically thick samples and samples with intrinsically high optical densities for which conventional classical transmission spectroscopy techniques may show limitations. The role of even-order dispersion compensation is specific to HOM interferometers. Classical spectroscopy does not benefit from such compensation. Therefore, HOM interferometers offer more accurate time resolution without having to account for some dispersion factors.

It is important to have the appropriate theoretical formalism to analyze the observed results from an HOM interaction, and we believe the lack of understanding on how to interpret this light−matter interference signal has set back the implementation of this spectroscopic method. As the light−matter interactions are encoded in the field correlations, the entangled biphoton state and sample transmission are used to obtain electric field operators of the photon mode through the sample, and this along with the beam splitter transformation is used to determine the coincidence counting rate. The counting rate depends on the joint spectral amplitude (JSA) which relates to the pump pulse and phase-matching function of the SPDC photons. This JSA, $f(\omega_s\omega_i)$, determined by the bandwidth and frequency of the pump and the properties of the nonlinear crystal, encodes the correlation between the frequencies of the SPDC photon modes (ω_s and ω_i).

As depicted in Figure 1b, a femtosecond laser is used as the pump in SPDC generation with a type II SPDC BBO crystal. The entangled photon pair (signal and idler beams) are separated by a polarizing beam splitter. A molecular sample is placed in the signal photon beam and a delay line in the idler photon beam, before the two beams recombine at a beam splitter and coincidence is measured. A theoretical framework for linear spectroscopic signals with an HOM setup is presented and specialized to this setup; the coincidence counting rate ($R_c(\tau)$) as a function of the optical delay τ between the two photon beams is given by[36]

$$R_c(\tau) = A\int_{-T_w/2}^{T_w/2} \mathrm{d}t\langle d^\dagger(t)c^\dagger(t+\tau)c(t+\tau)d(t)\rangle$$
$$= A\left(\frac{1}{2} - \frac{1}{2}\iint \mathrm{d}\omega\ \mathrm{d}\omega' f^*(\omega,\omega')f(\omega',\omega)\mathrm{T}^*(\omega')T(\omega)\mathrm{e}^{i(\omega-\omega')\tau}\right) \quad (1)$$

where $f(\omega',\omega)$ is an amplitude of the two-photon wave function (see eq 4) and $T(\omega)$ is a matter transition amplitude, which contains susceptibility (see eq 5). T_w is the detection window, and the constant A depends on the incoming photon flux, the efficiency of the photon detectors, and propagation losses. $c(\omega)$, $d(\omega)$ ($c^\dagger(\omega)$, $d^\dagger(\omega)$) are the boson annihilation (creation) operators corresponding to the photon modes detected by the two-photon detectors of the coincidence signal. The transmission function $T(\omega) \approx 1 + i\omega L\tilde{n}(\omega)/c$ for the signal photon arm encoding the matter influence on the transmitted field, with $\tilde{n}(\omega)$ the complex refractive index of matter, L the sample thickness, and c the speed of light. Integrating over frequencies in eq 1 corresponds to "blind" detectors, which detect photons of all frequencies. Equation 1 reveals how the matter modulates the coincidence count rate;

https://doi.org/10.1021/jacs.1c02514
J. Am. Chem. Soc. 2021, 143, 9070−9081

an intuitive way to understand this is that the effective JSA after interacting with matter is $f(\omega_s,\omega_i)T(\omega_s)$. In addition to the JSA which relates to the light field, the coincidence rate depends on the sample's susceptibility. Therefore, the coincidence rate contains matter information. From this connection between the matter properties and the HOM coincidence rate, it is possible to use the obtained HOM signal to determine optical properties of the molecule. As the signal contains the full linear susceptibility of the molecule, we utilize this to directly extract the molecule's dephasing time upon coherence excitation.

II. EXPERIMENTAL SECTION

Our experimental setup (Figure 1b) consists of entangled photons generated by using a mode-locked 800 nm Ti:sapphire laser (Spectra-Physics MaiTai) with 100 fs pulses at a repetition rate of 80 MHz. A 400 nm beam is produced via second harmonic generation (SHG) with a 1 mm thick β-barium borate (BBO) crystal. The power after SHG is set by using a neutral density filter on a translation stage. This 400 nm beam is subsequently used to pump a 1 mm BBO crystal cut for type II SPDC. The generated photon pairs have orthogonal polarizations and are frequency degenerate ($\omega_s = \omega_i$) with a half-opening angle of 5°. The SPDC crystal is placed in a rotating holder, such that the angle of the crystal with respect to the beam can be tuned to alter the phase-matching direction. The angle is then positioned to set the phase-matching orientation to collinear, such that the SPDC rings are "touching". A pinhole aperture is used to select the central overlap portion of the SPDC rings in the collinear phase-matching arrangement. A spatial arrangement of SPDC is confirmed by imaging with a CCD camera (Diffraction Limited STF-402M). After SPDC generation, any spurious 400 nm light is filtered out with a dichroic mirror and an interference filter (12 nm transmission centered at 800 nm). The 12 nm filter was used for initial scans to obtain the dip, since a narrower filter leads to better depth.[40]

At the input of the HOM interferometer system (Figure 1c), the entangled photons interact with a polarizing beam splitter creating two pathways: one for the signal photons and one for the idler. After the beams are separated, a time delay is created in one arm of the interferometer by using parallel quartz wedges placed on a motorized translation stage (Thorlabs MTS25), with resolution <0.5 fs (0.1 μm). This delay is adjusted by increasing the thickness of the quartz wedge through which the beam passes. A quartz plate is placed in the second arm of the interferometer to compensate for any disparity in the lengths of the two paths. A sample (or solvent) in a 2 mm path length quartz cuvette is placed in this second arm (which does not have the delay line). The mirror in arm 2 after the sample is mounted on a stepper motor controller translation stage (Thorlabs LNR25ZFS) to allow micrometer precise alignment of the length of the two beam paths. The entangled photon pairs from the two arms of the interferometer then recombine and interfere on a 50/50 beam splitter. After recombination, any information regarding polarization of the light is erased with polarization analyzers at the transmission and reflection output ports of the beam splitter, set at 45° relative to the incoming rays to maintain indistinguishability. The beams are focused onto the photosensitive area of single photon avalanche photodiodes (PerkinElmer SPCM-AQR-13) which are connected to a coincidence counting module (Ortec NIM7400, 10 ns coincidence window) to detect the photon rate in coincidences. Coincidence counts are measured as a function of time delay to obtain the HOM dip.

Because the 800 nm SPDC light is in the infrared range and not visible to the eye, an external visible He−Ne laser (not shown) was used to aid the alignment process. It is necessary that the beams from both paths are aligned both spatially and angularly to ensure a perfect overlap (at the beam splitter and at the detectors) and indistinguishability. With the He−Ne laser, the reflection of the beams exiting the final beam splitter can be projected onto a note card or a wall, and discrepancies in the beams' positions can be better observed. Once the beams overlap and the translation stage is set to the correct zero delay position, interference fringes should be discernible to confirm that the interferometer is well aligned. The He−Ne laser can then be removed for the SPDC light beam to travel through the setup to the detectors and coincidence scans to be measured as a function of time delay. Before HOM delay scans were performed, polarization visibility tests were performed to determine the degree of polarization entanglement of the SPDC light to ensure that entanglement is high enough for indistinguishability to be seen in the HOM measurements. In this test, the polarization analyzer at one detector is kept constant while the other analyzer is adjusted, and coincidence counts are measured as a function of this polarizer angle, showing where there is maximum entanglement. The graph of polarization visibility is shown in the Supporting Information (S1) and shows a visibility of 90 ± 2%, which is an appropriate value for measurements.

Two chromophores were used in this study: one with no one-photon absorption at 800 nm and another with an absorption peak resonant with the 800 nm entangled photons. The well-known and commercially available dye Coumarin 30 with absorption at ∼415 nm is used as the off-resonant sample and a control measurement. The main molecular system investigated is the dye IR-140 (Figure S2a) as its maximum absorption at 800 nm (Figure S2b) makes it an ideal resonant medium with the entangled photon spectrum. The sample has a single absorption peak with a broad spectrum from ∼700 to 850 nm. While a 12 nm interference filter was used for initial scans, because of the broad absorption band of the molecule, an interference filter with a 40 nm transmission was used for scans with solvent and sample to ensure there is an adequate overlap between the spectra of the entangled photons and the sample.

III. RESULTS AND DISCUSSION

The typically narrow bandwidth of the SPDC type II photons[41] is on the order of ∼10−20 nm. In our experiments the spectrum of the SPDC field is determined by the transmission curve of the interference filter used after SPDC to block out the remaining pump beam. Furthermore, the HOM depth is better with a filtered spectrum to reduce distinguishability.[42] Thus, to first observe the HOM dip, an interference filter centered at 800 nm with a FWHM of 12 nm is utilized for alignment. With this, the HOM dip is characterized as seen in Figure 1d showing the normalized coincidence counts as a function of time delay. The photons of the SPDC entangled pair travel separate but equal pathways and impinge on the beam splitter from opposite sides. The probability amplitudes of the paths with both transmitted, "t−t", and both reflected, "r−r", have the same amplitude but different relative phases. Thus, since it is impossible to distinguish the photons in these paths, they destructively interfere, leading to a drop in coincidence counts at zero delay when the indistinguishable photons overlap perfectly in time. A unitary transformation (which will be discussed in more detail) occurs at the output channels of the beam splitter and projects the input state of the photons into a N00N state where both photons of the entangled biphoton pair exit the beam splitter from the same output port. This superposition of the biphoton pair causes the signature bunching effect as a result of the bosonic properties of photons.[43]

Shown in Figure 1d are direct normalized coincidence counting measurements with no corrections or subtractions as a function of the time delay. The visibility is on the order of 40%. While imperfections in the visibility can be caused by factors in alignment and background events related to mixed states and two-photon components that do not interfere,[44] correlations have been drawn between the spectral properties of the SPDC photons and the resulting visibility. The broader

https://doi.org/10.1021/jacs.1c02514
J. Am. Chem. Soc. 2021, 143, 9070−9081

joint spectrum width of type II SPDC using ultrafast pulsed laser systems compared to pumping with CW lasers or using type I SPDC has been shown both theoretically and experimentally to reduce the quantum interference visibility of the HOM dip due to the large range of frequencies and wave vector modes.[41,45−48] An investigation on the effect of spectral information and distinguishability in type II SPDC with a broadband pump showed that as the pump bandwidth is increased, the overlap between the pump envelope and the phase-matching function also increases, leading to a larger range of frequencies in the downconverted photons and therefore greater distinguishability and lower visibility.[49] They were able to integrate an equation for the coincidence rate of the HOM counts, where $R_c(\delta\tau) \propto \sigma$ (where σ is proportional to the pump bandwidth) shown in eq 2.[49] For the CW pump limit, $\sigma \to 0$, therefore the coincidence rate at the dip can go to zero. Alternatively, as σ increases and the beams become more distinguishable, the lowest coincidence rate also increases and the visibility is diminished. Using smaller crystal lengths (≤0.5 mm) as well as narrow spectral filters can improve visibility,[48] and their calculations showed a visibility of ∼20−25% with an 8 nm filter, in line with our result with a 12 nm filter. Previous experimental studies have obtained HOM visibilities with ultrafast pumped type II SPDC photons in the range 20−30% for SPDC crystal thicknesses greater than 0.5 mm, which is consistent with our results.[45−47] This equation that roughly estimates the dependence of HOM visibility based on pump bandwidth is[49]

$$R_c(\delta\tau) \propto \frac{1}{\sqrt{2\pi}}\frac{\sigma}{\Omega_+} - \mathrm{erf}\left[\frac{1}{2\sqrt{2}}\frac{\sigma}{\Omega_+}(1 - |\delta\tau|\Omega_-)\right] \quad (2)$$

where σ is proportional to the pump bandwidth and $\Omega_\pm$ relates to the crystal length and phase matching conditions. Using this relation, we simulated the coincidence rate as a function of relative time delay for different pump bandwidths (see graphs with normalized coincidence rates simulated for different bandwidths in Figure S3 of the Supporting Information): a narrow bandwidth to simulate a CW laser (Figure S3a) and 8 times that bandwidth to simulate our femtosecond pump (Figure S3b). The narrow bandwidth of CW produces a visibility of ∼96%. This portrays the CW limit where $\sigma \to 0$, and the frequencies of the photon pair overlap perfectly in a narrow range. From the graph, it is clear that with this narrower bandwidth the HOM dip can be closer to perfect visibility as the photon pairs are more indistinguishable. However, for the spectrally wider femtosecond pump ($8\sigma_{CW}$), the visibility is much smaller and estimated to be ∼40% (the erf function in eq 2 accounts for the shape). The broader pump spectrum causes a spectral width which includes a distribution of frequencies. As such, the indistinguishability is reduced, causing lower visibility like the 40% calculated (Figure S3b). This is in accordance with our own experimental results. Clearly, the pump bandwidth plays a role on the HOM dip obtained and should be taken into consideration. For future experiments, a CW laser can be used to improve visibility.

The dip shown in Figure 1d has the characteristic symmetrical triangular or V-shape that is expected as described by theory.[50] The joint spectral function for type II SPDC, $S(\upsilon)$, within the SPDC state is commonly written as[48,51]

$$S(\nu) = \left|\mathrm{sinc}\left(\frac{\nu DL}{2}\right)\varepsilon_p(\omega_s + \omega_i)\right|^2 \quad (3)$$

where $\varepsilon_p(\omega_s + \omega_i)$ is the pump envelope, D represents the group velocity difference of the o and e polarized photons in the crystal ($D = \frac{1}{u_o} - \frac{1}{u_e}$), L is the thickness of the SPDC crystal, and ν is the detuning frequency of the signal and idler photons from half the pump frequency. The sinc function leads to the natural rectangular shape of the two-photon effective wave function, the Fourier transform of which produces the triangular shape of the HOM dip that can appear Gaussian from distortions due to the interference filter.[50] The experimental HOM dip (Figure 1d) is clearly symmetrical, with steady coincidence counts from ∼±800−400 fs, which peak before starting to drop, referencing the zero-delay point and indistinguishability and temporal correlation of the photon pairs. The coincidence counting rate of the HOM dip can also be written as $R_c(\tau) = R_0[1 - V(\tau)]$,[51] where R_0 is the coincidence rate at long delay times beyond any region of quantum interference and $V(\tau)$ has a dependence on DL. The parameters DL determine the entanglement time of the entangled photon pair, so it is expected that the width of the HOM dip should reflect this.

A spectral filter with a bandwidth smaller than the bandwidths of the individual photons causes an increase in their coherence time,[42] and thus the contribution of the spectral filtering can be used to estimate the broadened coherence time and subsequent dip width.[51] The HOM dips using both 12 and 40 nm interference filters are shown in Figure S4. The dip with the 12 nm filter is shown in red while that with the 40 nm filter is in black. There is a clear difference in the visibilities and widths of the two dips. Both dips are roughly triangular in shape, with counts stable around the maximum value from ∼±800 to ±400 fs before starting to descend to the zero-delay position. The zero-delay position is the same for both dips, indicating that the filter does not result in any phase changes or change the dip position. Narrowband filters may contribute to broadened coherence times while broader filters will result in narrower coherence times as the two-photon wavepacket is no longer spectrally filtered. In addition, by use of spectral filters with broader bandwidths, there is a higher possibility of detecting uncorrelated photons with a large frequency difference. This can cause significant accidental coincidence counts[51] which will reduce the quantum interference visibility.[52] Thus, using broader filters may result in lower visibilities than narrower bandwidth interference filters. This is reflected in the fitting of these dips taking into consideration the different filter widths (Figure S5). The filter is modeled by a Gaussian transmission function $T(\omega) = e^{-(\omega-\omega_0)^2/\sigma^2}$ where σ is the spectral width.

As the length and group velocity properties of the SPDC crystal are known, the entanglement time of the biphoton pair is calculated to be 126 fs, which would result in a coherence time and width of the dip of ∼255 fs as the FWHM of the dip represents the inverse of the bandwidth of the SPDC spectrum and the coherence time of the entangled photons. With the 12 nm interference filter, the filtered entanglement time is estimated to be 177 fs.[51] Therefore, the estimated coherence time of 2 times the entanglement time ($2T_e$) would be 354 fs, which agrees well with the coherence time of ∼370 fs obtained by the HOM dip with the 12 nm filter. Similarly, a 40 nm filtered dip without solvent is shown overlaid in the same graph. It is clear that due to the increased spectral width, the broader range of frequencies reduces the indistinguishability, and as such there is a smaller visibility with the 40 nm filter.

https://doi.org/10.1021/jacs.1c02514
J. Am. Chem. Soc. 2021, 143, 9070−9081

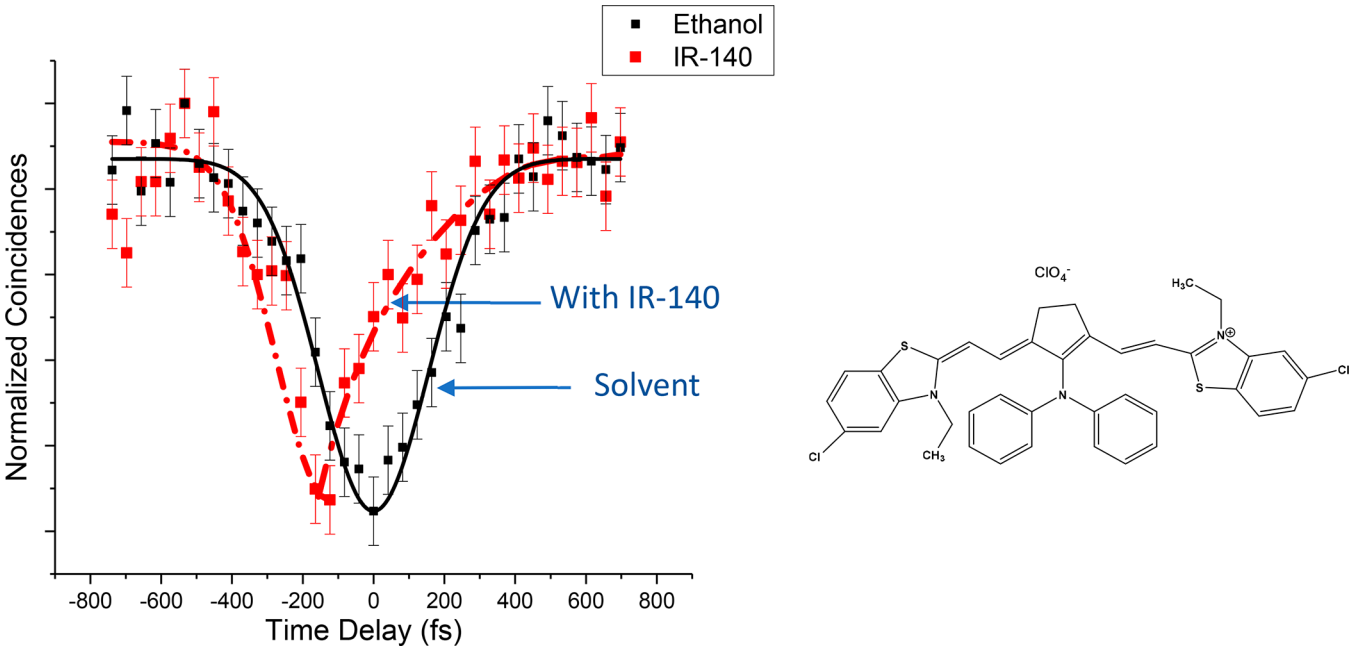

Figure 2. Normalized coincidence counts as a function of time delay showing the HOM dip without the sample (black) and the HOM dip with the IR-140 sample (red) and IR-140 structure.

Furthermore, the dip is visibly narrower than that used with the 12 nm filter. In fact, the coherence time from the HOM dip width is ~270 fs, which is in line with what is expected with no filter in place. This confirms that the SPDC spectrum is within 40 nm as it is no longer spectrally filtered by this additional interference filter which is why we do not see a considerably narrowed dip. It also confirms the entanglement time of the SPDC photon pair experimentally agrees with the 126 fs calculated time. For further experiments, the 40 nm interference filter was used with a 2 mm quartz cuvette with solvent placed in the interferometer path, causing slight broadening to the dip in further graphs albeit narrower than with the 12 nm filter (Figure 2).

The experiment is performed with a solvent (ethanol) as the control measurement and with IR-140 (dissolved in ethanol), a dye with strong absorption at 800 nm, as the resonant sample. The solutions are held in a 2 mm quartz cuvette which is placed in the beam path in one arm. In both cases (solvent and sample), the broader interference filter with a transmission bandwidth of 40 nm was used to overlap with the broad absorption band of IR-140. The HOM dip with solvent placed in the interferometer path is measured and the normalized coincidence rate as a function of time delay shown in Figure 2 (black curve). Again, the HOM dip with pure solvent is symmetric with a triangular almost Gaussian shape. There are steady counts on both ends peaking before counts drop, signifying the zero-delay position. There is a smooth decline of the counts to the zero-delay point, and the photons propagating through the ethanol do not get absorbed or experience interference with it.

The solvent is then replaced with the IR-140 dye (was 20.4 μM concentration), and the HOM scan is performed. With the sample in place, the features of the dip change, and the HOM dip becomes distorted as seen in Figure 2 (red curve). The left side of the dip is similar to that of the solvent scan, maintaining a Gaussian shape with coincidence counts peaking and then beginning to drop at ~400 fs. However, the dip overall becomes narrower and gains an asymmetry on the right side. The right side of the dip becomes almost inverted compared to the solvent scan until it reverts to steady coincident count levels. The side of the dip is no longer smooth, and there are multiple peaks or oscillations, with amplitude changes of ~7% within an 80 fs time window. Furthermore, the center of the HOM dip with the sample is shifted to the left compared to the dip with the solvent. Because the sample absorbs at 800 nm and interacts with only one photon of the entangled pair, this is a resonant one-photon process that involves linear excitation. This experiment was repeated with Coumarin 30, which is an off-resonant sample with no 800 nm absorption, and the HOM dip did not show a shift or change in shape (see the Supporting Information). As expected with the IR-140 dye, the photons that propagate through the resonant sample induce a coherent excitation that lasts for some time period. This interaction with the sample affects the phase of the photons that were transmitted through it and hence affects their quantum interference when recombined with the photons from the opposite path. As the light now possesses information related to the sample, this information is portrayed in the HOM dip and results in the subsequent shift and asymmetry that are now observed. It is very interesting that the organic molecule in the interferometer path results in changes to the shape and symmetry of the dip itself and not just a shift of the dip as a function of delay time. A simple shift in time with the same shape and symmetry is seen in polarization mode dispersion measurements to determine the refractive indices of optics. However, in this case the complexity of the distortions to the dip suggest more information about the molecule is accessed and present in the coincident count results. We are then interested in what molecular information can be extracted from the new shape and features obtained.

To understand the HOM interference process and how it is affected by the introduction of a resonant medium, we develop a theoretical formalism to describe the experiment. We first

https://doi.org/10.1021/jacs.1c02514
J. Am. Chem. Soc. 2021, 143, 9070−9081

consider the entangled biphoton twin state generated by SPDC. This can be described by

$$|\Phi\rangle = \iint d\omega_s\, d\omega_i f(\omega_s, \omega_i) a_s^{\dagger}(\omega_s) a_i^{\dagger}(\omega_i) |0_s, 0_i\rangle \tag{4}$$

where $f(\omega_s,\omega_i) = \alpha(\omega_s + \omega_i)\beta(\omega_s - \omega_i)$ is the joint spectral amplitude with $\alpha(\omega_s + \omega_i)$ as the pump envelope and $\beta(\omega_s - \omega_i)$ as the phase-matching function and where $a_s^{\dagger}(\omega)$, $a_s(\omega)$ [$(a_i^{\dagger}(\omega)$, $a_i(\omega)$] are the creation and annihilation operators, respectively, for the signal [and idler] modes. These satisfy the boson commutation relation $[a_j(\omega), a_j^{\dagger}(\omega')] = \delta(\omega - \omega')$. The signal mode is modified by interacting with the medium placed in the path; the modifications can be described by either a perturbative treatment or a continuum of lossy beam splitters.[36,53] After transmission through the sample, the signal mode operator $a_s(\omega)$ becomes

$$a_s'(\omega) = T(\omega) a_s(\omega) + \eta(\omega) \tag{5}$$

where $T(\omega)$ in the first term is the transmission function for the medium the light propagates through and $\eta(\omega)$ is the quantum noise associated with the absorption process. This transmission function, $T(\omega) = e^{i\omega(n(\omega)+i\kappa(\omega))L/c}$ (L is the sample length and c the speed through a vacuum), is determined by the dielectric constant (ϵ) (or linear susceptibility (χ)) of the medium. The complex refractive index of the sample satisfies the equality

$$(n(\omega) + i\kappa(\omega))^2 = \epsilon(\omega) = 1 + \chi(\omega) \tag{6}$$

The real part of this complex index adds a phase to the signal operator while the imaginary part contains the absorption (attenuation) by the medium. A wave packet of modes transmits through the sample, causing a modulation of the signal as it propagates through the sample which leads to the subsequent phase shift. It is clear from the expression in eq 6 how the transmission function is related to the dielectric constant and linear susceptibility. For a nonresonant and nonabsorbing medium that is transparent to the propagating photon $T(\omega) \approx 1$, and the signal mode operator remains almost unchanged. However, for a resonant absorbing medium, the signal mode interferes with the sample and therefore undergoes a phase shift and attenuation as dictated by the complex refractive index. For thin samples, the noise term in eq 5 can be neglected. Therefore, rewriting eqs 5 and 6 with the transmission function in terms of electric field operators, the electric field operators of the photon mode transmitted through the sample is

$$E^{(+)}(\omega) \equiv T(\omega) E_0^{(+)}(\omega) = E_0^{(+)}(\omega) + \frac{i\omega L}{c} \tilde{n}(\omega) E_0^{(+)}(\omega) \tag{7}$$

After the signal beam is transmitted through the sample, it recombines with the idler beam (which passed through the other arm of the HOM interferometer) at the 50:50 beam splitter. The idler beam undergoes a controllable phase shift, $a_i'(\omega) = a_i(\omega)\, e^{i\omega\tau}$ due to the travel path difference of the two beams. The output modes of the beam splitter, described by the photon operators $c(\omega)$ and $d(\omega)$, after this recombination are given by the 50:50 beam splitter unitary transformation:

$$\begin{pmatrix} c(\omega) \\ d(\omega) \end{pmatrix} = \frac{1}{\sqrt{2}} \begin{pmatrix} 1 & i \\ i & 1 \end{pmatrix} \begin{pmatrix} a_s'(\omega) \\ a_i'(\omega) \end{pmatrix} \tag{8}$$

This beam splitter unitary transformation introduces a $\pi/2$ phase shift in the reflected photons output state. The exiting beams travel to photodetectors and are measured in coincidence where the coincidence counting rate reads as eq 1, where we have used eq 8 in the first line and eq 5 in the second line of eq 1. The detectors are blind to the frequency of the photons; thus, the counting rate is integrated over frequency, and the coincidence counts depends on the phase of the photons. Equation 1 shows that the HOM signal provides a product of the spectral $f(\omega_s,\omega_i)$ and material $T(\omega_s)$ properties. This can be analyzed further by conducting a Fourier transform of eq 1. The Fourier transform of the signal in eq 1 yields

$$R(\Omega) = -\frac{1}{2}\beta^*(\Omega)\beta(-\Omega) T^*\left(\bar{\omega} - \frac{\Omega}{2}\right) T\left(\bar{\omega} + \frac{\Omega}{2}\right) \tag{9}$$

where $\bar{\omega} = {}^1/_2(\omega_1 + \omega_2)$. Again, there is a product of the spectral and material properties. When the signal and idler modes are broadband, eq 9 builds a connection between the Wigner transform of the transmission function and the coincidence counting rate (see the Supporting Information).

Because of the $T(\omega)$ function in the coincidence rate in eq 1, the resulting coincidence rate contains the full linear susceptibility of the absorbing medium in the interferometer path. Given that the beam transmitted through the sample is in resonance with some excited state of the sample, it creates a coherent excitation which must dephase over a time, T_2, governed by the group delay contribution. If the molecular response is dominated by a single resonance at Ω with dephasing time T_2, these can be linked to the linear susceptibility by a Lorentzian model for a two-level system as

$$\chi(\omega) = \frac{\alpha}{\omega - \Omega - i/T_2} \tag{10}$$

where α is a constant related to the length and concentration of the sample. By connecting our understanding of the HOM experimental data to the theoretical formalism and the susceptibility, we will be able to model our data to extract this dephasing time.

For comparison with our experimental data from the HOM experiment, the full susceptibility can be computationally simulated from the absorption data by using the Kramers–Kronig dispersion relation.[54] The imaginary part of the linear susceptibility $\chi''(\omega)$ is obtained by a Hilbert transform of $\chi''(\omega)$, $\chi'(\omega) = \frac{1}{\pi}\mathcal{P}\int_{-\infty}^{\infty} \frac{\chi''(\omega')}{\omega' - \omega}$ where $\mathcal{P}$ denotes the Cauchy principal value. A Gaussian joint spectral amplitude function

$$f(\omega_1, \omega_2) = (2\pi\sigma_p\sigma_-)^{-1/2} \exp[-(\omega_s + \omega_i - \omega_p)^2 / (16\sigma_p{}^2)] \exp[-(\omega_s - \omega_i)^2/(4\sigma_-{}^2)] \tag{11}$$

is used to fit the experimentally obtained HOM spectrum, which, along with the linear susceptibility, ensures the exact information the experimental data contain about the SPDC spectrum and the molecule studied. Here, σ_p is the bandwidth of the pump laser and $\sigma_- \propto 1/T_e$. ω_s, ω_i, and ω_p are the frequencies of the signal, idler, and pump, respectively.

With this study, we aim to provide the first step in illustrating that entangled photons in an HOM interferometer can be utilized for complex spectroscopy with organic, biological materials, and more, as the interferometer is sensitive to their presence and the SPDC two-photon wave function experiences a transformation caused by the sample's trans-

https://doi.org/10.1021/jacs.1c02514
J. Am. Chem. Soc. 2021, 143, 9070−9081

mission. Specifically, if our experiment can be modeled by using the linear susceptibility as expected by simulation and with this our experimental data can be used to extract time-resolved data pertaining to the molecule, it substantiates the viability of the HOM interference as a spectroscopic method to be studied further. Our objective is to understand how our HOM scan can be connected to the coherent excitation of the sample, which will be useful toward testing the feasibility of this spectroscopic method in more complex designs, with possibilities for time-resolved nonlinear spectroscopy with entangled photons.

First, the full linear susceptibility is simulated by using the Kramers−Kronig relation to fit to our signal from the HOM experiment. The computed linear susceptibility $\chi(\omega)$ of the IR-140 molecule from the absorption data is shown in Figure S5 constructed by computing a transformation on the imaginary part of the susceptibility. To fit the HOM dip obtained with the solvent in the interferometer arm, the coincidence counting rate in eq 1 and the Gaussian JSA in eq 11 are used, setting the transmission function $T(\omega)$ equal to 1. In this limit, there is no absorption by the medium and hence no attenuation or change to the phase of the propagating photon. By fitting the HOM data without the sample, we can obtain the full joint spectral amplitude of our SPDC source using eq 11 with the pump central frequency, ω_p = 1.549 eV, and bandwidth, σ_p = 23 meV. The central frequencies for the signal and idler photons are $\omega_s = \omega_i = \frac{\omega_p}{2}$. Hence with the fitting, the width σ_- is determined and found to be σ_- = 4 meV. This width, which is related to the SPDC photons as $\sigma_- \propto 1/T_e$, gives the diagonal of the JSA obtained (Figure 3a). The full JSA gives us

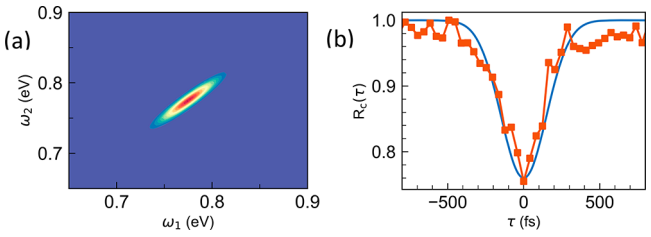

Figure 3. (a) Joint spectral amplitude $|f(\omega_s,\omega_i)|$ obtained by fitting eq 11 to the experimental HOM coincidence counting rate with solvent only. (b) Comparison between theory and experimental data for the HOM coincidence counting rate for the solvent only. Theoretical modeling is shown in blue.

a theoretical model of the SPDC two-photon amplitude and is shown in Figure 3a. This is important as it provides the width of the difference of the two modes of the biphoton pair and, thus, an understanding of the bandwidth and diagonal of the JSA and the frequency correlations of our SPDC source. As shown, the entangled signal and idler modes are correlated in their frequency. The width in the diagonal matches the pump bandwidth, where the off-diagonal width is determined by the phase-matching condition. Subsequently, the fitting of the HOM dip through solvent is simulated, and the comparison between the experimental HOM spectrum with only the solvent and theoretical modeling is depicted in Figure 3b. As shown, the fit produces a symmetric Gaussian shape through the HOM dip that descends toward the zero-delay position and peaks at ∼±500 fs. The FWHM of this fit is ∼375 fs, which is very similar to that obtained directly from the experimental data. Thus, the theory is in good agreement with the experiment and can assuredly be used for further analysis with the data involving the sample.

It is important to obtain a fitting of our experimental HOM data through the sample with the computed $\chi(\omega)$ and the full JSA of our entangled light source to confirm that the experiment does indeed agree with and contain the full information about the real and imaginary linear susceptibility, dephasing, and SPDC source. This will be necessary for extracting the dephasing time, T_2. The transmission function $T(\omega)$ in $R_c(\tau)$ is replaced with the real transmission from the linear susceptibility $\chi(\omega)$ of the sample. As the transmission through the resonant sample IR-140 showed attenuation of the coincidence counts while transmission through the non-resonant sample Coumarin 30 showed no attenuation at all, it is clear that there is absorption of the signal photons by the resonant IR-140 sample and a subsequent excitation of this sample despite the low entangled photon intensity. Conversely, Coumarin 30 is transparent to the light. The real transmission along with the full JSA obtained from fitting the solvent data is used to model the HOM spectrum with the IR-140 chromophore. Shown in Figure 4 is the theoretical fitting of

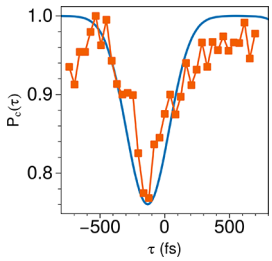

Figure 4. Comparison between theory and experimental data for the HOM coincidence counting rate for the IR-140 molecule.

the HOM coincidence count rate for the IR-140 molecule. Again, the theory is in good agreement with the experimental data. The theoretical fit reproduces the shift of the HOM dip, to the left of the original zero-delay position. Intuitively, the molecules act as a frequency-dependent phase shifter, which induces a phase shift in the signal photon beam $a(\omega)e^{i\theta(\omega)}$. The interbeam time delay can either compensate or amplify the relative difference between the two beams depending on the relative sign of τ and $\theta(\omega)$. This leads to a shift of the center of the dip, and it can be seen in Figure 4 that the dip with the sample is shifted to ∼−150 fs compared to the dip with the solvent. As the light−matter interference cannot be completely compensated by only the delay in the idler, in addition to the shift, there is an asymmetry of the HOM signal. The right side of the dip becomes elongated and asymmetrical compared to the left, representing the change in phase of the photons propagated through the sample in comparison to those in the opposite arm of the interferometer. This elongation is a reflection of the additional oscillations caused by the induced polarization of the molecule and the resulting effect in the propagating photons leading to a change in shape of the HOM dip. Thus, the exchange symmetry between the arms is broken. Evidently, our experimental data accurately reflect what is expected from theory. The ability to obtain the asymmetry in the modeled HOM dip depends on the form of the joint spectral amplitude (JSA) used in the simulations. Therefore, the asymmetry in the modeling is not as significant as that seen in the experimental data possibly as a result of the idealized

https://doi.org/10.1021/jacs.1c02514
J. Am. Chem. Soc. 2021, 143, 9070−9081

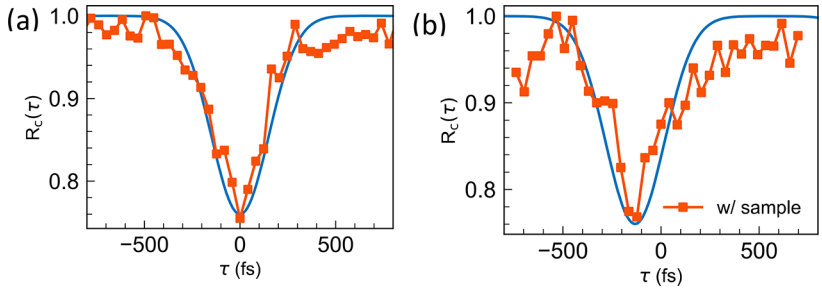

Figure 5. (a) HOM dip with solvent (without substance) and (b) HOM dip using the Lorentzian model for the IR-140 sample. These fits were modeled by using eq 10.

Gaussian form of the JSA. Therefore, by utilizing a more exact JSA such as one with a sinc form, the asymmetry seen in the experimental data may become more pronounced in the theoretical modeling. The agreement between the theoretical fit, which contains the IR-140 transmission data, and the experimental HOM data confirms that this IR-140 transmission information is indeed measured by the HOM interferometer.

The indistinguishability and temporal correlation of the photon pairs are advantageous, as the absorbing media in the interferometer path experience quantum interference with the signal photon of the entangled pair but not the idler. Therefore, because of its group velocity, the sample modulates the phase packet that propagates through it, and upon recombination with the idler photons, the signal photons hold information about the absorbing media which translates to an alteration of the interference between the entangled photon pair at the beam splitter and a change in the observed HOM dip. This expected result is successfully obtained by our experiment. As the signal measurements are conducted through coincidence counts and it is the statistics of the coincidences and not simply the photon intensity that is considered, they are a reflection of the entangled light photon statistics, therefore governed by nonclassical properties. One may think to attribute these changes to some simple refractive distortion caused by placing an additional optical element in one path of the interferometer. However, by conducting scans using solvent and the off-resonant Coumarin 30 dye with the same experimental parameters and same cuvette, it is clear that the observed result is substance-dependent. If the resonant absorption peak was shifted, off-center from resonance or nonresonant, this would most likely affect the observed HOM dip and the effect would not be as strong. There would be no shift of the dip or change in the HOM signal. Therefore, it is necessary that majority of the resonance peak overlaps with the measurement spectrum. The experiment delay time is shown at 40 fs increments and can be measured at as low as 4 fs as determined by the precision and increments of the delay stage used. Additionally, coincidence counts remained the same for scans using solvent and the Coumarin 30 dye, signifying no absorption but dropped for the IR-140 dye, which confirms that there was one photon absorption taking place.

Our main objective is to obtain molecular information from the data, specifically the dephasing time of the molecule's coherent excitation. As mentioned, the linear susceptibility can be connected to the dephasing time and the molecule's coherent excitation by the Lorentzian function in eq 10. Therefore, the HOM data can be exploited to obtain the dephasing time as was similarly considered in a previous study with a crystal and nanostructures.[37] We fit our experimental data using the Lorentzian model in eq 10. This simulation was done for both the HOM scans with and without the sample. The simulation of the HOM dip without the sample (with solvent) is shown in Figure 5a with the transmission again set to 1 to signify no absorption through the medium. The resulting fit is similar to the theoretical fit of $R_c(\tau)$ in Figure 3b, where the dip symmetrically descends to the zero-delay position with the ends flattening out at large delay times. The modeling provides the characteristic triangular almost Gaussian shape of the HOM dip, which confirms the width (time) and shape of the biphoton.

The graph in Figure 5b shows the Lorentzian modeling of the HOM data with the IR-140 sample in the interferometer path using eq 10, fit with the full linear susceptibility from transmission through the sample. This is very similar to the graph in Figure 4 simulated with $R_c(\tau)$ of eq 1. It is interesting that similar fittings can be achieved with eq 10, which contains mainly data pertaining to the sample such as the linear susceptibility, length, concentration, and resonance frequency as well as the frequency of the SPDC light. As the equation is heavily substance dependent, the ability to obtain a good fitting with it certifies that the experimental data through the sample contains molecular related information. The coherent excitation of the sample is successfully captured by the photons interferometric response and clearly seen in the alteration of the HOM dip and its simulated fitting.

The important aspect of this Lorentzian fitting is the ability to use it to connect the HOM data to time-resolved information pertaining to the sample. While current entangled light spectroscopy methods such as entangled two-photon absorption offer insights to nonlinear effects on dipole properties, many researchers across fields are interested in utilizing the temporal correlations of entangled photon pairs to measure temporal photophysical properties of substances under study. From the fitting in Figure 5b, we can extract the dephasing time T_2. Using the best fit of eq 10, we extracted the dephasing time of the IR-140 molecule and found to be ∼102 fs. Considering the broad line width of the IR-140 absorption band, we did expect to see a short coherence time, on the order of tens of femtoseconds. 102 fs is relatively short compared to times found with similar methods;[37] thus, it is an adequate result taking into consideration the line width broadening and the instrument entanglement time. The group delay contribution from the sample does not last long as is evident by the width of the oscillating asymmetric tail in the modified HOM dip. As such, we did not expect a long dephasing time and the extracted T_2 adequately reflects this. However, other techniques have been able to obtain a range of

https://doi.org/10.1021/jacs.1c02514
J. Am. Chem. Soc. 2021, 143, 9070−9081

dephasing times of IR-140 and similar dyes, sometimes shorter than our extracted value.[55−58] For example, a T_2 of 50 fs has been found with a degenerate four-wave mixing (DFWM) technique.[55] DFWM is a very involved process using multiple optics components, and very high concentrations of ∼1.7 × 10^{-4} M are used due to the high possibility of photobleaching with lower concentrations. These high concentrations could increase the possibility of aggregation and scattering which can lead to distortions of the measured dephasing times. Other studies that have been able to provide dephasing times of similar dyes on the same order of magnitude (30−60 fs) use either involving methods similar to DFWM such as photon echo[56] or use methods that require multiple wavelengths such as absolute Raman cross-section analysis.[57] To obtain multiple wavelengths for a single experiment, high-technology laser systems are needed which may not be available to all. Another study that looked at the dephasing time of IR-140[58] found that it would be at most 100 fs, similar to our obtained T_2, but was able to measure a time faster than that. As is it is possible that some overestimation is possible in our measurement, further studies using this inexpensive and easy assembly HOM spectroscopy method can conduct experiments with shorter entanglement times which will make deconvolution easier to extract even quicker dephasing times. Although our SPDC spectrum is much narrower than the molecule's absorption line width, we can provide a fitting that resolves a relatively short dephasing time. We suggest that to extract even shorter dephasing times for broad line width samples, the optical thickness of the sample could be adjusted as this may affect the line width and make extraction of coherence time more difficult. A smaller entanglement time (much shorter than the dephasing time) will also lead to simpler deconvolution of different broadening effects. Additionally, type I SPDC and continuous wave pump sources lead to higher HOM visibilities, making it easier to deduce subtle changes in coincidence counts and leading to more accurate data extraction. We suggest a type I SPDC source may be applied in future investigations. In the future, we also hope to conduct experiments with thin film samples to overcome hindrances by sample optical thickness.

Thus, our HOM interferometer is indeed sensitive to the presence of a resonant sample placed in its path. Our experiment provides a proof-of-concept illustration of an entangled photon spectroscopic method and is the first time this is illustrated with a chemical system. The experimental results along with theoretical fitting confirm that the coincidence counts measured by the HOM interferometer can be fit with the full (real and imaginary) linear susceptibility of a substance placed in its path and can be used to deduce the dephasing time T_2 of the chromophore even if it has a broad line width. The low photon flux of the entangled photons can induce an excitation in a resonant sample and our experimental method is sensitive to any observable changes. Therefore, this investigation of molecular properties using HOM interferometry presents itself as a viable method for conducting sensitive spectroscopy and opens the door for more complex spectroscopic design possibilities. The current setup can be readily extended to measuring higher-order nonlinear response functions (susceptibilities) of materials by using additional external classical laser pulses. These pulses can interact with the sample before the final interaction with the signal beam of the quantum light such that the transmitted beam carries information about the nonlinear susceptibilities of matter. This information can then be extracted by the coincidence counting measurements as demonstrated here. The coincidence counts will be able to capture fast evolving macroscopic and microscopic processes as a function of the time delay. Time-resolved signals can then be studied by controlling the temporal delay between the laser pulses. As we have corroborated the ability of this method to detect light−matter interactions, the next step is to perform such higher order experiments to capture excited-state dynamics on the samples under study, while taking advantage of the low flux, good signal-to-noise ratio, and control parameters of entangled light. Similarly, the frequency correlations, $f(\omega_s,\omega_i)$, can be varied by using different types of quantum light and observing the effects this has on the resulting light−matter interactions; the strength of the interference and coupling with different frequency correlations and the change to the observed phase shifts. By shaping the photon entanglement, we can manipulate the optical signals for different material responses. A vast array of material substances may be probed with this technique, particularly substances with interesting characteristics such as biological systems and quantum emitters. Single-photon emitters may be probed in a multiphoton interferometer regime to investigate higher order coherence characteristics by using low photon flux and strong temporal correlations.[59,60] Moreover, the experimental setup can be made easier to assemble and more accessible by using compact continuous wave lasers and type I SPDC, making this a highly resourceful experiment that many researchers can utilize across multiple fields. Nonlinear experiments that take advantage of the correlations and interferences of entangled photons with molecules have been proposed, and with this work, our experiment with HOM interferometry may be the doorway toward achieving these ideas and bringing them into fruition. Now the possibility to investigate a series of chromophores by using HOM interferometry to probe dynamical behavior upon coherent excitation has become a reality.

IV. CONCLUSIONS

We have successfully provided an experimental test of the sensitivity of entangled photons in an HOM interferometer to the presence of resonant organic dyes. We have been able to confirm that the coincidence counts and HOM dip are responsive to a resonant dye placed in the interferometer path and that the sample causes an interference and phase shift to the propagating photons. In accordance with our theory, the resulting HOM dip contains molecular information pertaining to the linear susceptibility and absorption of the studied sample. Mainly, the coincidence measurements of the HOM signal obtained from experiment can be connected to molecular dephasing and used to measure the molecular coherence times which is an important factor for further time-resolved studies. With our HOM experiment, we were able to extract a dephasing time of the organic molecule of as low as 102 fs upon coherent excitation and quantum interference with a path of entangled photons in the interferometer. This affirms the viability of HOM interferometry as a spectroscopic method to be used across scientific fields to study optical properties by using quantum advantages. There are numerous ways to advance this method for even more fascinating studies, and with our work, we have set the stage for these possibilities.

https://doi.org/10.1021/jacs.1c02514
J. Am. Chem. Soc. 2021, 143, 9070−9081

■ ASSOCIATED CONTENT

Supporting Information

The Supporting Information is available free of charge at https://pubs.acs.org/doi/10.1021/jacs.1c02514.

Polarization visibility test, materials, simulated visibility graphs for different pump bandwidths, nonresonant HOM scans, linear susceptibility plot and details on the limit of a narrowband pump and broadband photons (PDF)

■ AUTHOR INFORMATION

Corresponding Author

Theodore Goodson, III − *Department of Chemistry, University of Michigan, Ann Arbor, Michigan 48109, United States;* orcid.org/0000-0003-2453-2290; Email: tgoodson@umich.edu

Authors

Audrey Eshun − *Department of Chemistry, University of Michigan, Ann Arbor, Michigan 48109, United States*

Bing Gu − *Department of Chemistry & Department of Physics and Astronomy, University of California, Irvine, Irvine, California 92697, United States;* orcid.org/0000-0002-5787-3334

Oleg Varnavski − *Department of Chemistry, University of Michigan, Ann Arbor, Michigan 48109, United States*

Shahaf Asban − *Department of Chemistry & Department of Physics and Astronomy, University of California, Irvine, Irvine, California 92697, United States*

Konstantin E. Dorfman − *State Key Laboratory of Precision Spectroscopy, East China Normal University, Shanghai 200062, China*

Shaul Mukamel − *Department of Chemistry & Department of Physics and Astronomy, University of California, Irvine, Irvine, California 92697, United States;* orcid.org/0000-0002-6015-3135

Complete contact information is available at: https://pubs.acs.org/10.1021/jacs.1c02514

Notes

The authors declare no competing financial interest.

■ ACKNOWLEDGMENTS

T.G.III and S.M. acknowledge support from the U.S. Department of Energy, Office of Science, Office of Basic Energy Sciences, via Grant DE-SC0020168. T. G.III acknowledges support from the U.S. Air Force Office of Scientific Research in the Biophysics Program via Grant FA9550-20-1-0380. S.M. gratefully acknowledges the support by NSF Grant CHE-1953045. K.E.D. gratefully acknowledges the support from National Science Foundation of China (No. 11934011), Zijiang Endowed Young Scholar Fund, East China Normal University, and the Overseas Expertise Introduction Project for Discipline Innovation (111 Project, B12024).

■ REFERENCES

(1) Jennewein, T.; Simon, C.; Weihs, G.; Weinfurter, H.; Zeilinger, A. Quantum Cryptography with Entangled Photons. *Phys. Rev. Lett.* **2000**, *84* (20), 4729−4732.

(2) Lemos, G. B.; Borish, V.; Cole, G. D.; Ramelow, S.; Lapkiewicz, R.; Zeilinger, A. Quantum Imaging with Undetected Photons. *Nature* **2014**, *512* (7515), 409−412.

(3) Xu, W.; Wang, T.; Wang, C. Efficient Teleportation for High-Dimensional Quantum Computing. *IEEE Access* **2019**, *7*, 115331−115338.

(4) Chuan, X.; Zhang, L.; Huang, S.; Ma, T.; Liu, F.; Yonezawa, H.; Zhang, Y.; Xiao, M. Sensing and Tracking Enhanced by Quantum Squeezing. *Photonics Res.* **2019**, *7* (6), 14−26.

(5) Lee, D.; Goodson, T., III Entangled Photon Absorption in an Organic Porphyrin Dendrimer. *J. Phys. Chem. B* **2006**, *110*, 25582−25585.

(6) Guzman, A. R.; Harpham, M. R.; Suzer, O.; Haley, M. M.; Goodson, T. G., III Spatial Control of Entangled Two-Photon Absorption with Organic Chromophores¨. *J. Am. Chem. Soc.* **2010**, *132*, 7840−7841.

(7) Burdick, R. K.; Villabona-monsalve, J. P.; Mashour, G. A.; Goodson, T., III Modern Anesthetic Ethers Demonstrate Quantum Interactions with Entangled Photons. *Sci. Rep.* **2019**, *9*, 1−9.

(8) Villabona-monsalve, J. P.; Burdick, R. K.; Goodson, T. Measurements of Entangled Two-Photon Absorption in Organic Molecules with CW-Pumped Type - I Spontaneous Parametric Down- Conversion. *J. Phys. Chem. C* **2020**, *124*, 24526−24532.

(9) Harpham, M. R.; Goodson, T., III Thiophene Dendrimers as Entangled Photon Sensor Materials. *J. Am. Chem. Soc. Artic.* **2018**, *21*, 973−979.

(10) Upton, L.; Harpham, M.; Suzer, O.; Richter, M.; Mukamel, S.; Goodson, T. Optically Excited Entangled States in Organic Molecules Illuminate. *J. Phys. Chem. Lett.* **2013**, *4*, 2046−2052.

(11) Varnavski, O.; Pinsky, B.; Goodson, T. Entangled Photon Excited Fluorescence in Organic Materials: An Ultrafast Coincidence Detector. *J. Phys. Chem. Lett.* **2017**, *8*, 388−393.

(12) Eshun, A.; Cai, Z.; Awies, M.; Yu, L.; Goodson, T., III Investigations of Thienoacene Molecules for Classical and Entangled Two-Photon Absorption Published as Part of The Journal of Physical Chemistry Virtual Special Issue " William M. Jackson Festschrift. *J. Phys. Chem. A* **2018**, *122*, 8167−8182.

(13) Villabona-monsalve, J. P.; Varnavski, O.; Palfey, B. A.; Goodson, T., III Two-Photon Excitation of Flavins and Flavoproteins with Classical and Quantum Light. *J. Am. Chem. Soc.* **2018**, *140*, 14562−14566.

(14) Villabona-Monsalve, J. P.; Calderón-Losada, O.; Nuñez Portela, M.; Valencia, A. Entangled Two Photon Absorption Cross Section on the 808 nm Region for the Common Dyes Zinc Tetraphenylporphyrin and Rhodamine B. *J. Phys. Chem. A* **2017**, *121*, 7869−7875.

(15) Tabakaev, D.; Montagnese, M.; Haack, G.; Bonacina, L.; Wolf, J.-P.; Zbinden, H.; Thew, R. T. Energy-Time Entangled Two-Photon Molecular Absorption. *Phys. Rev. A: At., Mol., Opt. Phys.* **2021**, *103*, 1−5.

(16) Varnavski, O.; Goodson, T. Two-Photon Fluorescence Microscopy at Extremely Low Excitation Intensity: The Power of Quantum Correlations. *J. Am. Chem. Soc.* **2020**, *142*, 12966−12975.

(17) Kaiser, F.; Vergyris, P.; Aktas, D.; Babin, C.; Labonté, L.; Tanzilli, S. Quantum Enhancement of Accuracy and Precision in Optical Interferometry. *Light: Sci. Appl.* **2018**, *7* (3), 17163−17165.

(18) Israel, Y.; Rosen, S.; Silberberg, Y. Supersensitive Polarization Microscopy Using NOON States of Light. *Phys. Rev. Lett.* **2014**, *112*, 12−15.

(19) Armendáriz, G.; Cravioto-Lagos, J.; Velázquez, V.; Grether, M.; López-Moreno, E.; Galvez, E. J. Teaching Quantum Mechanics with the Hong-Ou-Mandel Interferometer. *SPIE* **2014**, *9289* (July), 928908.

(20) Thomas, P. J.; Cheung, J. Y.; Chunnilall, C. J.; Dunn, M. H. The Hong-Ou-Mandel Interferometer: A New Procedure for Alignment. *Rev. Sci. Instrum.* **2009**, *80* (3), 036101.

(21) Atatüre, M.; Sergienko, A. V.; Saleh, B. E. A.; Teich, M. C. Entanglement in Cascaded-Crystal Parametric down-Conversion. *Phys. Rev. Lett.* **2001**, *86* (18), 4013−4016.

(22) Jachura, M.; Chrapkiewicz, R. Shot-by-Shot Imaging of Hong−Ou−Mandel Interference with an Intensified SCMOS Camera. *Opt. Lett.* **2015**, *40* (7), 1540.

(23) Li, H.; Piryatinski, A.; Jerke, J.; Kandada, A. R. S.; Silva, C.; Bittner, E. R Probing Dynamical Symmetry Breaking Using Quantum-Entangled Photons Probing Dynamical Symmetry Breaking Using Quantum-Entangled Photons. *Quantum Sci. amd Technol.* **2018**, *3*, 015003.
(24) Schlawin, F. Entangled Photon Spectroscopy. *J. Phys. B: At., Mol. Opt. Phys.* **2017**, *50*, 203001.
(25) Saleh, B. E. A.; Jost, B. M.; Fei, H.; Teich, M. C. Entangled-Photon Virtual-State Spectroscopy. *Phys. Rev. Lett.* **1998**, *80*, 3483−3486.
(26) Yabushita, A.; Kobayashi, T. Spectroscopy by Frequency-Entangled Photon Pairs. *Phys. Rev. A: At., Mol., Opt. Phys.* **2004**, *69*, 3−6.
(27) Dauler, E.; Jaeger, G.; Muller, A.; Migdall, A.; Sergienko, A. Tests of a Two-Photon Technique for Measuring Polarization Mode Dispersion With Subfemtosecond Precision. *J. Res. Natl. Inst. Stand. Technol.* **1999**, *104* (1), 1−10.
(28) Hong, S.; Riedinger, R.; Marinkovic, I.; Wallucks, A.; Hofer, S. G.; Norte, R. A.; Aspelmeyer, M.; Groblacher, S. Hanbury Brown and Twiss Interferometry of Single Phonons from an Optomechanical Resonator. *Science (Washington, DC, U. S.)* **2017**, *358*, 203−206.
(29) Hong, C. K.; Ou, Z. Y.; Mandel, L. Measurement of Subpicosend Time Intervals between Two Photons by Interference. *Phys. Rev. Lett.* **1987**, *59* (18), 2044−2046.
(30) Shih, Y. H.; Alley, C. O. New Type of Einstein-Podolsky-Rosen-Bohm Experiment Using Pairs of Light Quanta Produced by Optical Parametric Down Conversion. *Phys. Rev. Lett.* **1988**, *61* (26), 2921−2924.
(31) Walborn, S. P.; de Oliveira, A. N.; Pádua, S.; Monken, C. H. Multimode Hong-Ou-Mandel Interference. *Phys. Rev. Lett.* **2003**, *90*, 1−4.
(32) Lim, H. T.; Hong, K. H.; Kim, Y. H. Effects of Polarization Mode Dispersion on Polarization-Entangled Photons Generated via Broadband Pumped Spontaneous Parametric down-Conversion. *Sci. Rep.* **2016**, *6* (April), 1−7.
(33) Dorfman, K. E.; Schlawin, F.; Mukamel, S. Stimulated Raman Spectroscopy with Entangled Light: Enhanced Resolution and Pathway Selection. *J. Phys. Chem. Lett.* **2014**, *5*, 2843−2849.
(34) Mukamel, S.; Freyberger, M.; Schleich, W.; Bellini, M.; Zavatta, A.; Leuchs, G.; Silberhorn, C.; Boyd, R. W.; Sánchez-soto, L. L.; et al. Roadmap on Quantum Light Spectroscopy. *J. Phys. B: At., Mol. Opt. Phys.* **2020**, *53* (072002), 1−45.
(35) Chen, Y.; Fink, M.; Steinlechner, F.; Torres, J. P.; Ursin, R. Hong-Ou-Mandel Interferometry on a Biphoton Beat Note. *npj Quantum Inf.* **2019**, 1−6.
(36) Dorfman, K. E.; Asban, S.; Gu, B.; Mukamel, S. Hong-Ou-Mandel Interferometry and Spectroscopy Using Entangled Photons. *Commun. Phys.* **2021**, *4* (49), 1−7.
(37) Kalashnikov, D. A.; Melik-gaykazyan, E. V.; Kalachev, A. A.; Yu, Y. F.; Kuznetsov, A. I.; Krivitsky, L. A. Quantum Interference in the Presence of a Resonant Medium. *Sci. Rep.* **2017**, *7*, 1−8.
(38) Szoke, S.; Liu, H.; Hickam, B. P.; He, M.; Cushing, S. K. Entangled Light-Matter Interactions and Spectroscopy. *J. Mater. Chem. C* **2020**, *8*, 10732−10741.
(39) Graciano, P. Y.; Michel, A.; Martínez, A.; Lopez-Mago, D.; Castro-Olvera, G.; Rosete-Aguilar, M.; Garduño-Mejía, J. Interference Effects in Quantum- Optical Coherence Tomography Using Spectrally Engineered Photon Pairs. *Sci. Rep.* **2019**, *9*, 8954.
(40) Tanida, M.; Okamoto, R.; Takeuchi, S. Highly Indistinguishable Heralded Single-Photon Sources Using Parametric down Conversion. *Opt. Express* **2012**, *20* (14), 134−140.
(41) Kim, Y.; Grice, W. P. Measurement of the Spectral Properties of the Two- Photon State Generated via Type II Spontaneous Parametric Downconversion. *Opt. Lett.* **2005**, *30* (8), 908−910.
(42) Grice, W. P.; Erdmann, R.; Walmsley, I. A.; Branning, D. Spectral Distinguishability in Ultrafast Parametric Down-Conversion. *Phys. Rev. A: At., Mol., Opt. Phys.* **1998**, *57* (4), 2289−2292.
(43) Kambs, B.; Becher, C. Limitations on the Indistinguishability of Photons from Remote Solid State Sources Limitations on the Indistinguishability of Photons from Remote Solid State Sources. *New J. Phys.* **2018**, *20* (11), 115003.
(44) Cassemiro, K. N.; Laiho, K.; Silberhorn, C. Accessing the Purity of a Single Photon by the Width of the Hong−Ou−Mandel Interference. *New J. Phys.* **2010**, *12* (11), 1−15.
(45) Atature, M.; Di Giuseppe, G.; Shaw, M. D.; Sergienko, A. V.; Saleh, B. E. A.; Teich, M. C. Multiparameter Entanglement in Quantum Interferometry. *Phys. Rev. A: At., Mol., Opt. Phys.* **2002**, *66* (2), 1−15.
(46) Atature, M.; Di Giuseppe, G.; Shaw, M. D.; Sergienko, A. V.; Saleh, B. E. A.; Teich, M. C. Multiparameter Entanglement in Femtosecond Parametric Down-Conversion. *Phys. Rev. A: At., Mol., Opt. Phys.* **2002**, *65* (2), 1−4.
(47) Kim, Y.; Berardi, V.; Chekhova, M. V.; Shih, Y. Anticorrelation Effect in Femtosecond-Pulse Pumped Type-II Spontaneous Parametric down-Conversion. *Phys. Rev. A: At., Mol., Opt. Phys.* **2001**, *64*, 1−4.
(48) Kim, Y.; Grice, W. P. Generation of Pulsed Polarization-Entangled Two-Photon State via Temporal and Spectral Engineering. *J. Mod. Opt.* **2002**, *49* (14), 2309−2323.
(49) Grice, W. P.; Walmsley, I. A. Spectral Information and Distinguishability in Type-II down-Conversion with a Broadband Pump. *Phys. Rev. A: At., Mol., Opt. Phys.* **1997**, *56* (2), 1627−1634.
(50) Takeuchi, S. Recent Progress in Single-Photon and Entangled-Photon Generation and Applications. *Jpn. J. Appl. Phys.* **2014**, *53*, 030101.
(51) Kim, Y. Measuerement of One-Photon and Two-Photon Wave Packets in Spontaneous Parametric Downconversion. *J. Opt. Soc. Am. B* **2003**, *20* (9), 1959−1966.
(52) Poh, H. S.; Lum, C. Y.; Marcikic, I.; Lamas-linares, A.; Kurtsiefer, C. Joint Spectrum Mapping of Polarization Entanglement in Spontaneous Parametric Down-Conversion. *Phys. Rev. A: At., Mol., Opt. Phys.* **2007**, *75*, 1−8.
(53) Loudon, R. *The Quantum Theory of Light*; Oxford University Press: 2000; pp 1−438.
(54) Lucarini, B. V.; Saarinen, J. J.; Peiponen, K.; Vartiainen, E. M. *Kramers-Kronig Relations in Optical Materials Research*; Physica-Verlag-Springer: 2005; pp 1−160.
(55) Liebig, C. M.; Dennis, W. M. Optical Dephasing in Saturable-Absorbing Organic. *Appl. Opt.* **2006**, *45* (9), 2072−2076.
(56) Becker, P. C.; Fragnito, H. L.; Bigot, J. Y.; Brito Cruz, C. H.; Fork, R. L.; Shank, C. V. Femtosecond Photon Echoes from Molecules in Solution. *Phys. Rev. Lett.* **1989**, *63* (5), 505−507.
(57) Li, B.; Myers, A. B. Cross Sections Tor Cyclohexane, Acetonitrile, and Water in the Far-Ultraviolet Region. *J. Phys. Chem.* **1990**, *94*, 4051−4054.
(58) Chachisvilis, M.; Fidder, H.; Sundstrom, V. Electronic Coherence in Pseudo Two-Colour Pump-Probe Spectroscopy. *Chem. Phys. Lett.* **1995**, *234*, 141−150.
(59) Schlawin, F.; Mukamel, S. Two-Photon Spectroscopy of Excitons with Entangled Photons. *J. Chem. Phys.* **2013**, *139* (24), 1−11.
(60) Gu, B.; Mukamel, S. Manipulating Two-Photon-Absorption of Cavity Polaritons by Entangled Light. *J. Phys. Chem. Lett.* **2020**, *11* (19), 8177−8182.

https://doi.org/10.1021/jacs.1c02514
J. Am. Chem. Soc. 2021, 143, 9070−9081

Supporting Information

Investigations of Molecular Optical Properties Using Quantum Light and Hong-Ou-Mandel Interferometry

*Audrey Eshun[‡]; Bing Gu[§]; Oleg Varnavski[‡], Shahaf Asban[§]; Konstantin E. Dorfman[†]; Shaul Mukamel[§]; Theodore Goodson III[‡**]*

Polarization Visibility Test

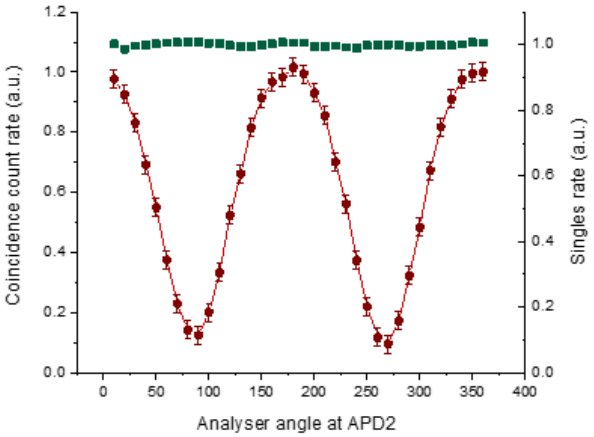

Figure S1. *Graph showing polarization visibility. Normalized coincidence count rate as a function of polarizer angle (red). Singles count rate as a function of polarizer angle (green).*

A polarization visibility test was conducted to determine the degree of polarization entanglement of the SPDC light to ensure that entanglement is high enough for indistinguishability to be seen in the HOM measurements. In this test, the polarization analyzer at one detector is kept constant while the other analyzer is adjusted, and coincidence counts are measured as a function of this polarizer angle, showing where there is maximum entanglement. When the polarizer angle at detector A is orthogonal to that at detector B, the maximum coincidence counts are observed, confirming the polarization entanglement of the photon pairs. Alternatively, when the polarization angles are the same, no coincidences are

detected since detector A does not register the twin photon of the entangled photon pair. Figure S1 shows a visibility of 90 ± 2%.

Materials

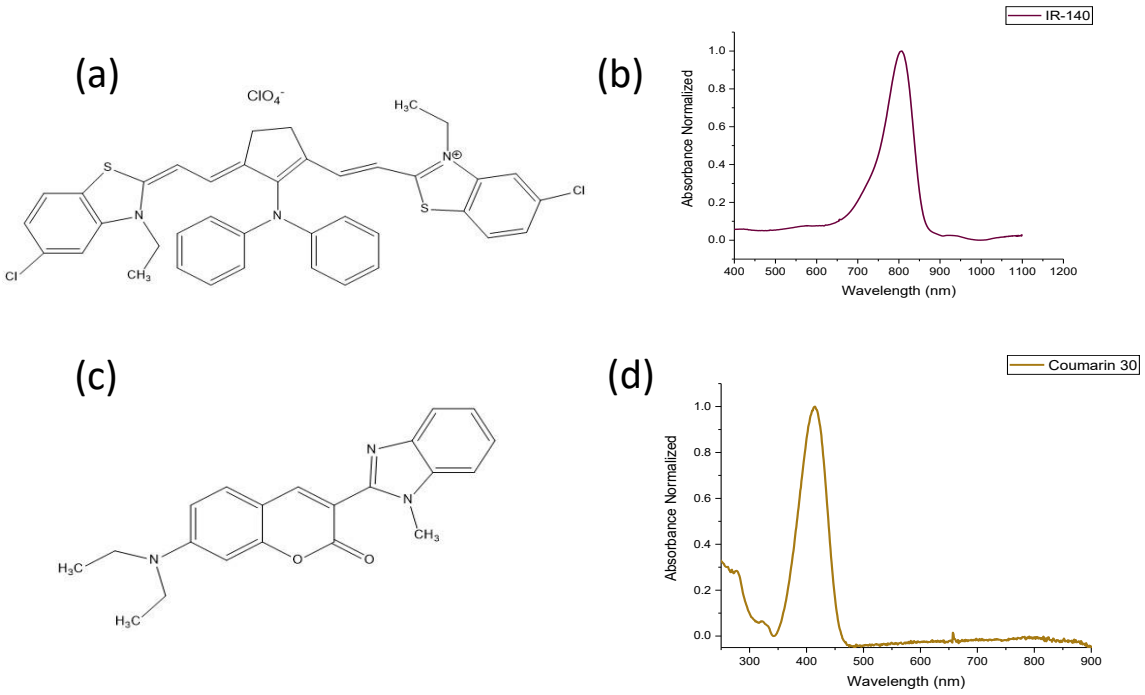

Figure S2. *(a) Molecular structure of IR-140. (a) Normalized absorption spectra of IR-140 dye. Concentration 20μM. (c) Molecular structure of Coumarin 30. (d) Normalized absorption spectra of Coumarin 30 dye. Concentration 29 μM.*

Simulated Visibility Depending on Pump Bandwidth

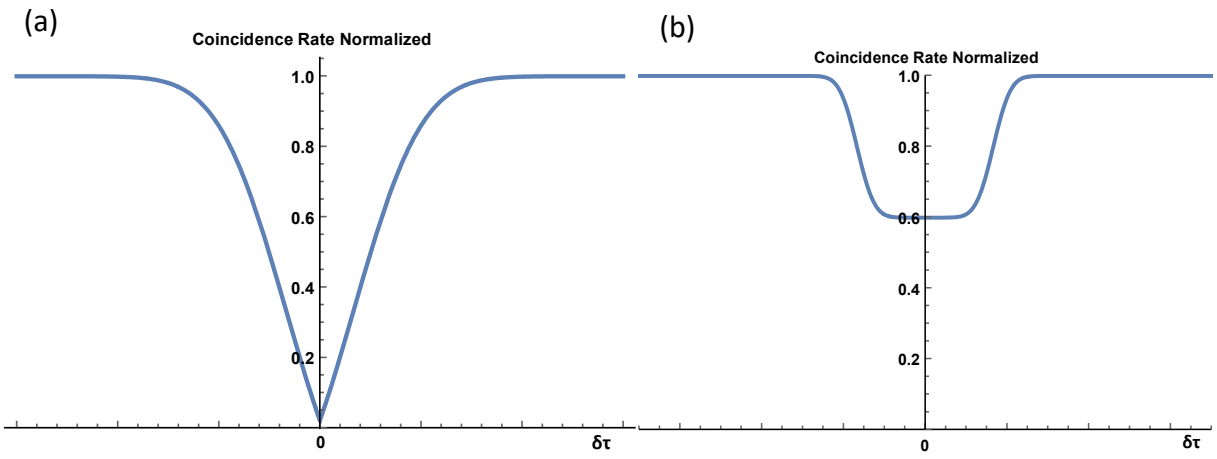

Figure S3. *Normalized coincidence rate as a function of time estimated using Eq. 2 for (a) a narrow CW pump bandwidth and (b) a larger femtosecond pump that is* $8\sigma_{CW}$.

HOM Scans with Interference Filter Dependence

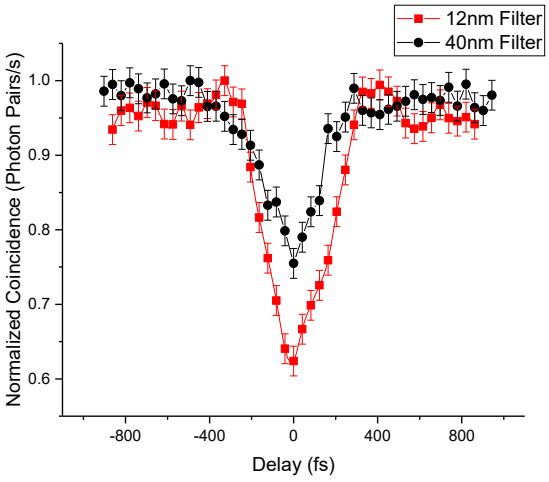

Figure S4. *HOM dips measured using 12nm interference filter (red) and 40nm interference filter (black).*

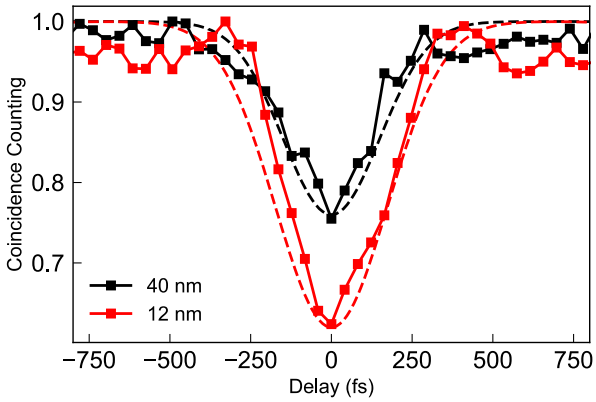

Figure S5*. Theoretically fitted HOM dips modelled with different joint spectral amplitudes which include the effects of interference filters.*

HOM Scans with Coumarin 30

The HOM dip with solvent (methanol) placed in the interferometer path is measured and the normalized coincidence rate as a function of time delay is shown in supplementary Fig. S6. Similar to the dip in Figure 3 of the main paper, the dip with solvent is symmetric and triangular, with steadily oscillating counts on both ends before counts drop, signifying the zero-delay position. The declining portion of the dip is smooth on both sides with no oscillations and any changes in amplitude as low as 1%. This reproduced symmetrical triangular shape confirms that the methanol does not absorb the photons or interfere with them and is not excited by them. Thus, methanol does not affect the two-photon quantum interference, and this serves as an accurate control scan.

Subsequently, the pure solvent in the interferometer arm was replaced with Coumarin 30 (dissolved in methanol). As Coumarin 30 has no absorption at 800nm, this was used to determine how the HOM dip would be affected by a non-resonant medium placed in the interferometer path. There was little to no change with the Coumarin 30 sample placed in the interferometer path (Fig. S6). The HOM dip maintains its symmetric triangular shape, with steady coincidence counts

oscillating at ± 2.5% on the ends before smoothly descending to the zero-delay position. In addition to the HOM dip maintaining its shape, the coincidence counts from the measurement with Coumarin 30 remain the same and display no attenuation compared to the counts with pure solvent. This indicates that the photons propagated through the non-resonant sample were not absorbed and did not interfere with the sample, thus there was no coherent excitation of the Coumarin 30 chromophore. The photons propagating through this dye experienced no new phenomena or phase change compared to the photons in the opposite path, therefore, upon recombining at the beam splitter there is no difference in their interaction and the HOM dip is unchanged. This was conducted with both 12 and 40nm filters to ensure that the broader filter did not result in a different outcome.

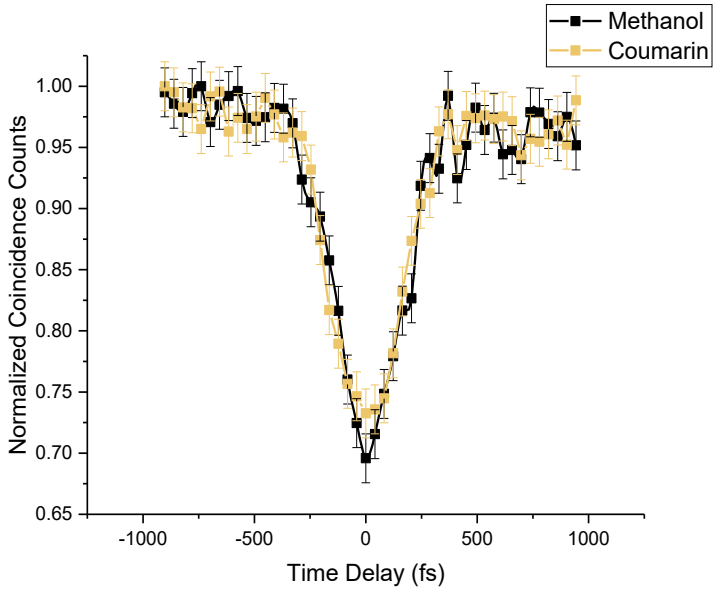

Figure S6. *Normalized coincidence counts as a function of time delay showing the HOM dip with a solvent, Methanol, (shown in black) and with a non-resonant sample, Coumarin 30 (shown in yellow).*

IR-140 linear Susceptibility

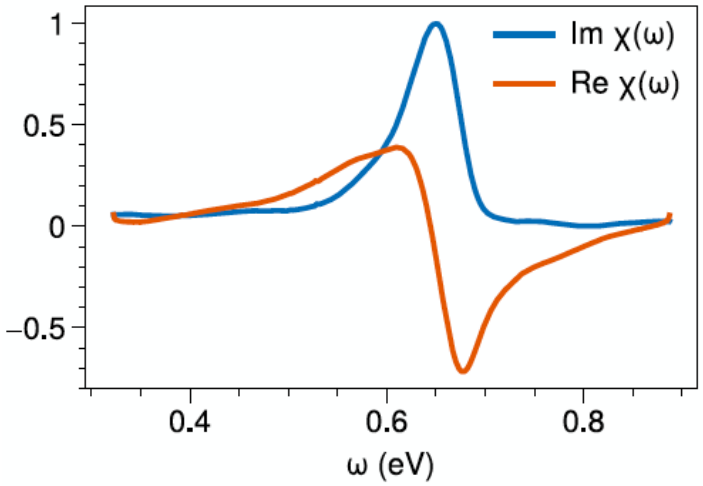

Figure S7*. Imaginary, Im $\chi(\omega)$, and real, Re $\chi(\omega)$, parts of the linear susceptibility of the IR-140 molecule The real part is obtained by Hilbert transform of the absorption data.*

Theoretical Modelling Overlaid

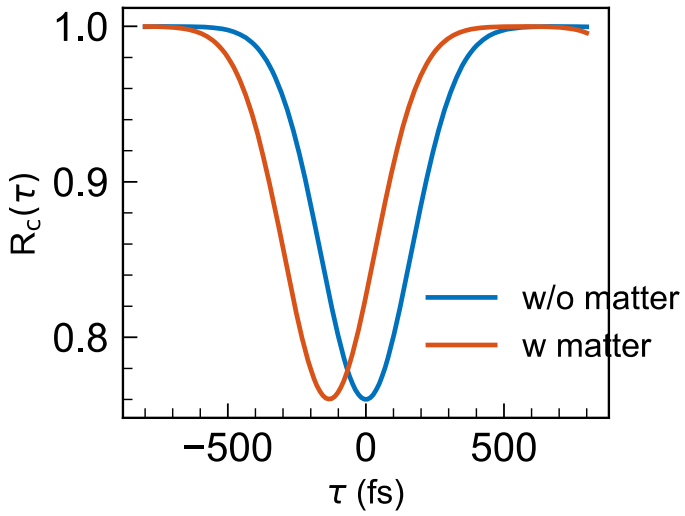

Figure S8*. Theoretical modelling of the HOM dips with and without sample overlaid.*

Narrowband pump and broadband twin photons

In the limit of a narrowband pump ($\sigma_+ \to 0$) and broadband twin photons (i.e. $\sigma_-$is larger than

the characteristic linewidth γ of the transmission function), Fourier transform of the HOM coincidence counting rate (Eq. 2) leads to

$$R(\tau) = -\frac{1}{2}\int d\Delta\beta^*(\Delta)\beta(-\Delta)T^*\left(\bar{\omega}-\frac{\Delta}{2}\right)T\left(\bar{\omega}+\frac{\Delta}{2}\right)e^{i\Delta\tau} = -\frac{1}{2}\int d\Delta\, T^*\left(\bar{\omega}-\frac{\Delta}{2}\right)T\left(\bar{\omega}+\frac{\Delta}{2}\right)e^{i\Delta\tau} \equiv -\frac{1}{2}T_W\left(\frac{\omega_p}{2},\tau\right) \quad \text{Eq. S1}$$

Eq. S1 shows that in this limit, the coincidence counting rate is determined by the Wigner transform of the transmission function. By scanning the pump frequency, it is possible to obtain the full $T_W(\omega,\tau)$. Note that the condition $\sigma_- \gg \gamma$ is not satisfied in the current experiment.

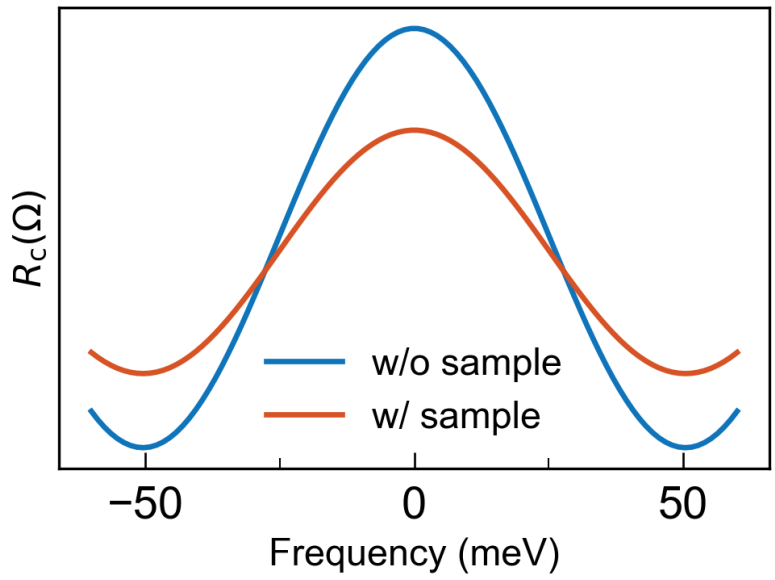

Figure S8*. Fourier transform of coincidence rates according to Eq. 8. We observe a difference in the frequency distributions and amplitude for the data with and without a sample.*